


**Absence of the FFLO/BCS hybrid paired ground state in superconducting Weyl semimetals**Jun Fang,<sup>1</sup> Chao Zhang<sup>2</sup>, and Zhongshui Ma<sup>1,3,\*</sup><sup>1</sup>*School of Physics, Peking University, Beijing 100871, China*<sup>2</sup>*School of Physics, University of Wollongong, New South Wales 2522, Australia*<sup>3</sup>*Collaborative Innovation Center of Quantum Matter, Beijing 100871, China* (Received 19 October 2022; revised 14 March 2023; accepted 12 April 2023; published 26 April 2023)

We study microscopic pairing mechanisms of superconductivity in doped Weyl semimetals. Depending on the nature of the electron scattering, there exist three possible superconducting pairings. We evaluate the condensation energy required for electrons to pair up. The ground state of superconducting Weyl semimetals is determined by the fermionic interaction. The scattering between two Weyl nodes plays an important role in pairing mechanisms. It is shown that the Fulde-Ferrell-Larkin-Ovchinnikov (FFLO) phase is the ground state if the electron scattering is dominated by the intranode scattering. On the other hand, if the internode scattering is strong, the ground state is with the BCS pairing. More importantly, we show that the state with FFLO/BCS hybrid pairing cannot be the ground state of superconducting Weyl semimetals, thus our result provides a definitive answer to an unresolved question.

DOI: [10.1103/PhysRevB.107.144512](https://doi.org/10.1103/PhysRevB.107.144512)**I. INTRODUCTION**

An important question in superconductivity is what type of interaction is responsible for electron pairing on the Fermi surface. Since the Weyl semimetal (WSM) has been predicted theoretically and realized experimentally [1–8], the research has focused on the unconventional pairing originating from disconnected Fermi surfaces in superconducting Weyl semimetals (SWSMs). In WSMs, there are an even number of nodal points, which are separated from each other, with different chiralities. Accordingly, the chemical potential intersects the band with an even number of disconnected Fermi surfaces (FSs). The nontrivial topological structure of FSs stimulated study on the superconducting mechanism in SWSMs [9–17]. Two superconducting pairings have been proposed for SWSMs: the intranode pairing and the internode pairing. The former is a pairing by electrons from the same node so that it is spatially nonuniform [18–20] and depends on the local momentum of Weyl nodes. The latter is a pairing by electrons from different nodes and is spatially uniform. The intranode pairing complies with the Fulde-Ferrell-Larkin-Ovchinnikov (FFLO) [9,18,19] mechanism, while the internode pairing corresponds to the BCS mechanism. It has been demonstrated that the SWSM with BCS pairing can have four nodal points in the energy spectrum. The bound state with a crossed flat surface can exist in SWSMs [16,17,21]. Theoretically, MoTe<sub>2</sub> was predicted to host four pairs of Weyl points [22]. The unconventional superconductivity in MoTe<sub>2</sub> has been validated experimentally [14].

Over the last few years, the ground states in SWSMs with the FFLO and BCS superconducting pairings have been

studied. Moore *et al.* [9] found the condensation energy of SWSMs with a FFLO-pairing mechanism has a lower value than that with a BCS-pairing mechanism. It is shown that the FFLO pairing appears in noncentrosymmetric systems where two Weyl nodes have different energies, while in BCS pairing, there is a mismatch in the electron momenta [23]. In contrast to Moore's result, Burkov *et al.* [13] show that the BCS pairing has a lower condensation energy if the inversion symmetry is not broken. What type of pairing is responsible for the superconductivity remains unsolved to date. Recently, to distinguish the ground state properties of SWSMs, hybrid structures combining SWSM and other materials are used to study the transport characteristics due to the FFLO and BCS pairing. The pairing-dependent Andreev reflection processes have been investigated in WSM/SWSM heterojunctions [24–26]. The SWSM Josephson junctions were proposed to exhibit features of the FFLO and the BCS ground state [27,28]. Gilbert *et al.* studied possible FFLO and BCS phase transition in magnetically doped time-reversal invariant topological insulators [29]. The result indicates that there might be a similar phase transition in the SWSM. Although there has been much effort to reveal the nature of the pairing mechanism in SWSMs and to develop possible measurement schemes for confirming particular features, the pairing mechanism in SWSMs remains inconclusive. The question of whether there exists a possibility of the state resulted from a coexistence of the FFLO and BCS orders, or a FFLO/BCS paired state, remains unresolved. We shall find an answer to this question in this work.

To resolve this issue, we investigate the energy required for electrons to pair up and the microscopic pairing mechanism. We shall identify the role of intra- and internode scattering on the conventional or unconventional pairing. Our starting point is the electron-electron interaction, where the potentials for both the intra- and the interpairings are present

\*Corresponding author: mzs@pku.edu.cn

[9,13]. We found that the gap equations have three solutions which correspond to three different superconducting pairings in SWSM. The ground state of SWSM is dependent on the interaction of electrons, specifically, the interaction strength with different scattering momentum. By analyzing the condensation energies for these three mechanisms, we show that the ground state is a FFLO state when the scattering between two Weyl nodes is weak. However, once the internode scattering becomes stronger than the intranode scattering, the BCS pairing becomes more favorable. We found that states with the FFLO/BCS hybrid pairing is also possible but cannot be the ground state of SWSM. This finding provides a definitive answer to the unresolved issue regarding this matter.

## II. INTRA- AND INTERNODE INTERACTIONS: FFLO AND BCS PAIRING HAMILTONIAN

We consider a WSM that breaks time-reversal symmetry but remains invariant under inversion, with an attractive interaction between electrons,  $H = H_0 + H_I$ , where  $H_0$  describes noninteracting electrons in WSM:

$$H_0 = \sum_{\kappa} \int d\mathbf{r} \psi_{\kappa}^{\dagger}(\mathbf{r}) [h_{\kappa}^e(-i\hbar\nabla) - \mu] \psi_{\kappa}(\mathbf{r}), \quad (1)$$

two Weyl nodes of opposite chirality separated by a distance  $b$  are located at  $\mathbf{P}_{\pm} = (0, 0, \pm b)$ ,  $\psi_{\kappa}(\mathbf{r}) = (\psi_{\kappa, \uparrow}(\mathbf{r}), \psi_{\kappa, \downarrow}(\mathbf{r}))^T$ ,  $h_{\kappa}^e(-i\hbar\nabla) = -i\hbar v_F \{\sigma_x \partial_x + \sigma_y \partial_y + \kappa \sigma_z [\partial_z - i(\kappa/\hbar)b]\}$ ,  $\mu$  is the chemical potential,  $\sigma_i$  ( $i = x, y, z$ ) are Pauli matrices,  $\hbar$  is Planck constant,  $\mathcal{T}$  means a transpose, and  $\kappa$  ( $= \pm$ ) stands for the chirality.  $H_I$  is the interaction between electrons, given as

$$H_I = - \int d\mathbf{r} d\mathbf{r}' U(\mathbf{r} - \mathbf{r}') \psi_{\uparrow}^{\dagger}(\mathbf{r}) \psi_{\downarrow}^{\dagger}(\mathbf{r}') \psi_{\downarrow}(\mathbf{r}') \psi_{\uparrow}(\mathbf{r}), \quad (2)$$

where  $U$  is interaction strength for the  $s$ -wave pairing and  $\psi_{\sigma}(\mathbf{r}) = \sum_{\kappa} (1/\sqrt{2}) \psi_{\kappa, \sigma}(\mathbf{r})$ .

In the momentum space, the field operator can be written as  $\psi_{\kappa, \sigma}(\mathbf{r}) = 1/\sqrt{V} \sum_{\mathbf{k}} e^{i\mathbf{k}\cdot\mathbf{r}} d_{\kappa, \mathbf{k}, \sigma}$ , where  $d_{\kappa, \mathbf{k}, \sigma}$  is the annihilation operator for the electron with momentum  $\mathbf{k}_{\kappa} = \mathbf{k} + \mathbf{P}_{\kappa}$ .  $\mathbf{k}$  is the momentum measured from the Weyl node  $\mathbf{P}_{\kappa}$ .  $\psi_{\kappa, \sigma}^{\dagger}(\mathbf{r})$  can be written in the same way but with a creation operator  $d_{\kappa, \mathbf{k}, \sigma}^{\dagger}$ . In  $d_{\kappa, \mathbf{k}, \sigma}^{\dagger}$  and  $d_{\kappa, \mathbf{k}, \sigma}$ ,  $H_0$  is given by

$$H_0 = \frac{1}{V} \sum_{\kappa, \mathbf{k}} \xi_{\kappa, \mathbf{k}}^{\dagger} [h_{\kappa}(\mathbf{k}) - \mu] \xi_{\kappa, \mathbf{k}}, \quad (3)$$

with  $h_{\kappa}(\mathbf{k}) = v_F(\sigma_x k_x + \sigma_y k_y + \kappa \sigma_z k_z)$  and  $\xi_{\kappa, \mathbf{k}} = (d_{\kappa, \mathbf{k}, \uparrow} \quad d_{\kappa, \mathbf{k}, \downarrow})^T$ .  $H_I$  is given as

$$\begin{aligned} H_I = & - \frac{1}{4V^2} \sum_{\kappa_1 \kappa_2 \kappa_3 \kappa_4} \sum_{\mathbf{k}_1 \mathbf{k}_2 \mathbf{k}_3 \mathbf{k}_4} U(\mathbf{k}_{1\kappa_1} - \mathbf{k}_{4\kappa_4}) \\ & \times \delta(\mathbf{k}_{1\kappa_1} + \mathbf{k}_{2\kappa_2} - \mathbf{k}_{3\kappa_3} - \mathbf{k}_{4\kappa_4}) \\ & \times d_{\kappa_1, \mathbf{k}_{1\kappa_1}, \uparrow}^{\dagger} d_{\kappa_2, \mathbf{k}_{2\kappa_2}, \downarrow}^{\dagger} d_{\kappa_3, \mathbf{k}_{3\kappa_3}, \downarrow} d_{\kappa_4, \mathbf{k}_{4\kappa_4}, \uparrow}. \end{aligned} \quad (4)$$

Assuming  $|\mathbf{P}_{\kappa}| \gg |k_i|$  ( $i = 1, 2, 3, 4$ ), the conservation of momentum and  $s$ -wave condition requires  $\mathbf{k}_1 + \mathbf{k}_2 = \mathbf{k}_3 +$

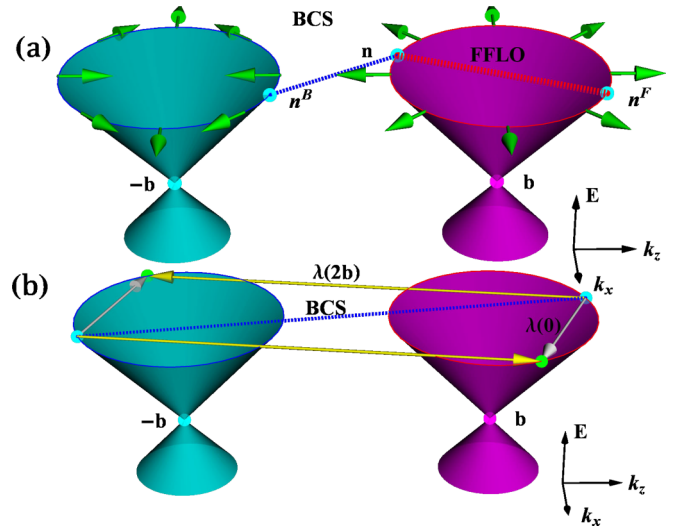


FIG. 1. (a) Sketch of BCS and FFLO pairing:  $n^F$  corresponds to the FFLO-type pairing electron and  $n^B$  corresponds to the BCS-type pairing electron. The green arrow is the direction of spin, and the red and blue circles are FS. (b) The scattering for the BCS interaction (yellow arrow): the intranode scattering potential is  $\lambda(0)$ , while the internode scattering (silver arrow) potential is  $\lambda(2b)$ .

$\mathbf{k}_4 = 0$  and  $\kappa_1 + \kappa_2 = \kappa_3 + \kappa_4$ .  $H_I$  can then be written as

$$\begin{aligned} H_I = & - \sum_{\kappa_1 \kappa_2 \kappa_3 \kappa_4} \sum_{\mathbf{k}, \mathbf{k}'} \frac{U(|\mathbf{P}_{\kappa_1} - \mathbf{P}_{\kappa_4}|)}{4V^2} \delta_{\kappa_1 + \kappa_2, \kappa_3 + \kappa_4} \\ & \times d_{\kappa_1, \mathbf{k}_{\kappa_1}, \uparrow}^{\dagger} d_{\kappa_2, -\mathbf{k}_{\kappa_2}, \downarrow}^{\dagger} d_{\kappa_3, -\mathbf{k}'_{\kappa_3}, \downarrow} d_{\kappa_4, \mathbf{k}'_{\kappa_4}, \uparrow}, \end{aligned} \quad (5)$$

where  $-\mathbf{k}_{\kappa} = -\mathbf{k} - \mathbf{P}_{\kappa}$ .

Under the restriction of  $\delta_{\kappa_1 + \kappa_2, \kappa_3 + \kappa_4}$ , there are two possible pairing channels with  $\kappa_i$  ( $i = 1, 2, 3, 4$ ). (1)  $\kappa_1 = \kappa_2 = \kappa_3 = \kappa_4$  which corresponds to the pairing taking place in the same node (FFLO pairing), and (2)  $\kappa_1 + \kappa_2 = \kappa_3 + \kappa_4 = 0$ , corresponding to the BCS pairing. Figure 1(a) shows pairing fermions in the two nodes. For a Cooper pairing in an anisotropic superconducting state, the magnitude  $U(\mathbf{k})$  varies slowly in the momentum space and can be regarded as relatively fixed in the vicinity of Weyl nodes. The situation is different for the pairing interaction between the nodes. The distance between two Weyl points is  $|\mathbf{P}_{\kappa_1} - \mathbf{P}_{\kappa_4}| = 2\delta_{\kappa_1, -\kappa_4} b$ . The pairing interaction  $U(|\mathbf{P}_{\kappa_1} - \mathbf{P}_{\kappa_4}|)$  can be written as  $U(0)$  for the FFLO pairing and  $U(2\delta_{\kappa_1, -\kappa_4} b)$  for the BCS pairing. Therefore,  $H_I$  consists of two types of terms:  $H_I^F$  and  $H_I^B$ , where  $H_I^F$  contains the product of components with the same momentum shift related to the node  $H_I^F = - \sum_{\kappa} \sum_{\mathbf{k}, \mathbf{k}'} \lambda(0) d_{\kappa, \mathbf{k}, \uparrow}^{\dagger} d_{\kappa, -\mathbf{k}, \downarrow}^{\dagger} d_{\kappa, -\mathbf{k}', \downarrow} d_{\kappa, \mathbf{k}', \uparrow}$  and  $H_I^B$  contains the Cooper pairing channel with zero total momentum  $H_I^B = - \sum_{\kappa, \kappa'} \sum_{\mathbf{k}, \mathbf{k}'} \lambda(2\delta_{\kappa, -\kappa'} b) d_{\kappa, \mathbf{k}, \uparrow}^{\dagger} d_{-\kappa, -\mathbf{k}, \downarrow}^{\dagger} d_{-\kappa', -\mathbf{k}', \downarrow} d_{\kappa', \mathbf{k}', \uparrow}$ , where the  $b$ -dependent factor is  $\lambda(2\delta_{\kappa, -\kappa'} b) = U(2\delta_{\kappa, -\kappa'} b)/4V^2$ . Figure 1(b) shows the effect on electron scattering. The Fourier components of a four-fermion interaction weakens slowly in momentum space so that  $\lambda(0) > \lambda(2b)$  if  $|\mathbf{P}_{\kappa}| \gg |\mathbf{k}_i|$ . For the short-range interaction,  $\lambda(0) \simeq \lambda(2b)$ .

### III. GAP EQUATION

We now introduce a unitary transformation  $\eta_{\kappa, \mathbf{k}\kappa} = U_{\kappa}^{\dagger}(\mathbf{k})\xi_{\kappa, \mathbf{k}\kappa}$ , where  $U_{\kappa}(\mathbf{k}) = \begin{pmatrix} \cos(\theta_{\kappa}/2)e^{-i\phi/2} & \sin(\theta_{\kappa}/2)e^{-i\phi/2} \\ \sin(\theta_{\kappa}/2)e^{i\phi/2} & -\cos(\theta_{\kappa}/2)e^{i\phi/2} \end{pmatrix}$ ,  $\eta_{\kappa, \mathbf{k}\kappa} = (c_{\kappa, \mathbf{k}\kappa, +} \ c_{\kappa, \mathbf{k}\kappa, -})^T$ ,  $\theta_{\kappa} = \arccos \kappa k_z/k$ , and  $\phi = \arctan k_y/k_x$ . The subscript  $+$  ( $-$ ) refers to the up (down) energy band.  $H_0$  and  $H_I^{F/B}$  read  $H_0 = \sum_{\kappa, \gamma} \int d\mathbf{k}/(2\pi\hbar)^3 (\gamma v_F k - \mu) c_{\kappa, \mathbf{k}\kappa, \gamma}^{\dagger} c_{\kappa, \mathbf{k}\kappa, \gamma}$ ,  $H_I^F = -(1/4) \sum_{\kappa, \gamma} \int d\mathbf{k} d\mathbf{k}' / (2\pi\hbar)^6 \lambda(0) c_{\kappa, \mathbf{k}\kappa, \gamma}^{\dagger} c_{\kappa, -\mathbf{k}\kappa, \gamma}^{\dagger} c_{\kappa, -\mathbf{k}'\kappa, \gamma} c_{\kappa, \mathbf{k}'\kappa, \gamma}$ , and  $H_I^B = -(1/4) \sum_{\kappa, \kappa', \gamma} \int d\mathbf{k} d\mathbf{k}' / (2\pi\hbar)^6 \lambda(2\delta_{\kappa, -\kappa'}) b [A + B]$ , where  $A = \sin \theta \sin \theta' c_{\kappa, \mathbf{k}\kappa, \gamma}^{\dagger} c_{\kappa, -\mathbf{k}\kappa, \gamma}^{\dagger} c_{-\kappa', -\mathbf{k}'\kappa, \gamma} c_{\kappa', \mathbf{k}'\kappa, \gamma}$  is the intraband term describing the interaction between electrons from the up levels in two different Weyl nodes,  $B = \cos \theta \cos \theta' c_{\kappa, \mathbf{k}\kappa, \gamma}^{\dagger} c_{\kappa, -\mathbf{k}\kappa, \gamma}^{\dagger} c_{-\kappa', -\mathbf{k}'\kappa, \gamma} c_{\kappa', \mathbf{k}'\kappa, \gamma}$  is the interband term describing the electrons from the up band of node  $\kappa$  interacting with the electrons in the down level of node  $-\kappa$ ,  $\theta = \theta_+$ . The cross band scattering is weaker than the scattering within the same band. Therefore, the term  $B$  can be neglected in the lowest-order approximation.

We now solve the Eliashberg equations to determine which pairing is more stable energetically. By taking into account the FFLO and the BCS pairings in the Hamiltonian  $H = H_0 + H_I^F + H_I^B$ , the linearized Eliashberg equation in the weak-coupling approximation is given by

$$\Delta_F \equiv -\frac{\lambda(0)}{2} \int_D \frac{d\mathbf{k}'}{(2\pi\hbar)^3} \langle F_{\gamma}^{++}(k', 0) \rangle \quad (6)$$

and

$$\Delta_B \equiv -\sum_{\kappa} \frac{\lambda(2\delta_{\kappa, 1}b)}{2} \int_D \frac{d\mathbf{k}'}{(2\pi\hbar)^3} \sin \theta' \langle F_{\gamma}^{-\kappa\kappa}(k', 0) \rangle, \quad (7)$$

for the FFLO and the BCS pairings, respectively. Here  $\mathcal{F}_{\gamma}^{\kappa\kappa'}(\mathbf{k}, \tau - \tau') = c_{\kappa, \mathbf{k}\kappa, \gamma}^{\dagger}(\tau) c_{\kappa', -\mathbf{k}\kappa', \gamma}(\tau')$  and the subscript  $D$  means the integrations are restricted in the region around  $\mu$  scaled with Debye frequency  $\omega_D$  [30]. In the calculation, we take  $\Delta_{B/F}$  as positive real numbers and neglect their phase. We assume the pairing is isotropic and  $k$  independent. The Green's function  $\mathcal{G}_{\gamma}(\mathbf{k}, \tau - \tau') = -\langle T_{\tau} [\mathcal{G}_{\gamma}^{\kappa\kappa'}(\mathbf{k}, \tau - \tau')] \rangle$  and the correlation function  $\mathcal{F}_{\gamma}^{\kappa\kappa'}(\mathbf{k}, \tau - \tau') = \langle T_{\tau} [\mathcal{F}_{\gamma}^{\kappa\kappa'}(\mathbf{k}, \tau - \tau')] \rangle$  are obtained as the functions of momentum and Matsubara frequency  $\mathcal{G}_{\gamma}(\mathbf{k}, i\omega) = -[i\omega + (\gamma v_F k - \mu)] \Sigma_{\gamma}(\omega, \mathbf{k}) / \Omega_{\gamma}(\omega, \mathbf{k})$  and  $\mathcal{F}_{\gamma}^{\kappa\kappa'}(\mathbf{k}, i\omega) = -(\Delta_F - i \Delta_B \sin \theta \sigma_y) \Sigma_{\gamma}(\omega, \mathbf{k}) / \Omega_{\gamma}(\omega, \mathbf{k})$ , where  $\mathcal{G}_{\gamma}^{\kappa\kappa'}(\mathbf{k}, \tau - \tau') = c_{\kappa, \mathbf{k}\kappa, \gamma}(\tau) c_{\kappa', -\mathbf{k}\kappa', \gamma}(\tau')$ ,  $\Sigma_{\gamma}(\omega, \mathbf{k}) = \Xi_{+,+}^{\gamma}(\omega, \mathbf{k}) + i2\Delta_F \Delta_B \sin \theta \sigma_y$ ,  $\Omega_{\gamma}(\omega, \mathbf{k}) = [\Xi_{+,+}^{\gamma}(\omega, \mathbf{k})]^2 - 4\Delta_F^2 \Delta_B^2 \sin^2 \theta$ , and  $\Xi_{\eta, \xi}^{\gamma}(\omega, \mathbf{k}) = \omega^2 + (\gamma v_F k - \mu)^2 + \zeta(\Delta_F^2 + \eta \Delta_B^2 \sin^2 \theta)$ .

Using the relation  $\mathcal{F}_{\gamma}^{\kappa\kappa'}(k', \tau = 0) = \beta^{-1} \sum_{\omega_n} \mathcal{F}_{\gamma}^{\kappa\kappa'}(k', i\omega_n)$ , the self-consistent gap functions are obtained:

$$\Delta_F = \frac{\lambda}{2\beta} \int_D \frac{d\mathbf{k}}{(2\pi\hbar)^3} \sum_{\omega_n} \frac{\Delta_F \Xi_{-,+}^+(\omega_n, \mathbf{k})}{\Omega_+(\omega_n, \mathbf{k})} \quad (8)$$

and

$$\Delta_B = \frac{\lambda(1+\alpha)}{2\beta} \int_D \frac{d\mathbf{k}}{(2\pi\hbar)^3} \sum_{\omega_n} \frac{\Delta_B \sin^2 \theta \Xi_{-,+}^+(\omega_n, \mathbf{k})}{\Omega_+(\omega_n, \mathbf{k})}, \quad (9)$$

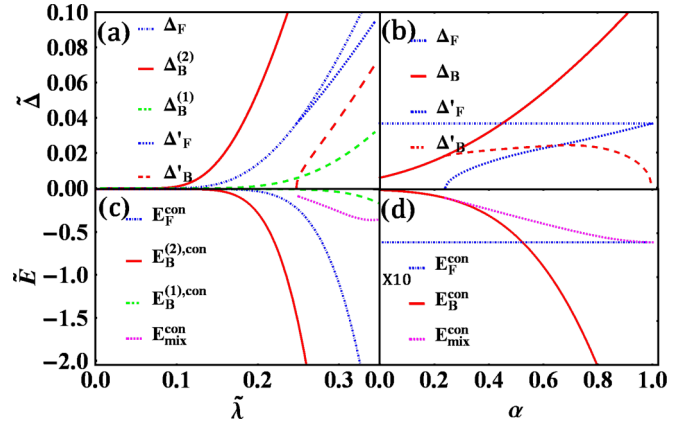


FIG. 2. Normalized energy gap and condensed energy. (a) Dependence of gap on  $\lambda$ :  $\Delta_F$  (blue dot-dashed),  $\Delta_B^{(2)}$  (red solid) for  $\alpha = 1$ ,  $\Delta_B^{(1)}$  (green dashed) for  $\alpha = 0$ ,  $\Delta_F'$  (blue short-dashed) for  $\alpha = 1$ , and  $\Delta_B'$  (red long-dashed) for  $\alpha = 1$ . (b) Change of gap function with  $\alpha$  at  $\lambda = C/4\mu^2$ :  $\Delta_F$  (blue dot-dashed),  $\Delta_B$  (red solid),  $\Delta_F'$  (blue short-dashed), and  $\Delta_B'$  (red long-dashed). (c) Dependence of condensed energy on  $\lambda$ :  $E_F^{\text{con}}$  (blue dot-dashed),  $E_B^{(2),\text{con}}$  (red solid) for  $\alpha = 1$ ,  $E_B^{(1),\text{con}}$  (green long-dashed) for  $\alpha = 0$ ,  $E_{\text{mix}}^{\text{con}}$  (magenta short-dashed) for  $\alpha = 1$ . (d) Change of condensed energy with  $\alpha$  at  $\lambda = C/4\mu^2$ :  $E_F^{\text{con}}$  (blue dot-dashed),  $E_B^{\text{con}}$  (red solid),  $E_{\text{mix}}^{\text{con}}$  (magenta short-dashed).

where  $\beta^{-1} = k_B T$ ,  $\lambda(0) = \lambda$ , and  $\lambda(2b) = \alpha\lambda$ ;  $\alpha \in [0, 1]$  is a parameter characterizing the relative strength of the BCS pairing interaction.

### IV. THREE POSSIBLE PAIRINGS

There exist three different solutions for Eqs. (8) and (9). (a)  $\Delta_F \neq 0$  and  $\Delta_B = 0$  (FFLO), (b)  $\Delta_B \neq 0$  and  $\Delta_F = 0$  (BCS), and (c)  $\Delta_F \neq 0$  and  $\Delta_B \neq 0$  (the FFLO/BCS hybrid). Figure 2 shows the results of the normalized energy gap ( $\tilde{\Delta} = \Delta/\omega_D$ ) and the normalized condensation energy ( $\tilde{E} = E/E_0$ ) where  $E_0 = 10^{-2} \mu^2 \Omega_D^2 / C$ . The normalized scattering potential is  $\tilde{\lambda} = \lambda(\mu^2/C)$ .

#### A. FFLO pairing

The gap function for pure FFLO pairing becomes independent of  $\theta$  and  $\alpha$ . Integrating  $k$  over a region around the Fermi surface with a width of  $\omega_D$  leads to an equation for  $\Delta_F$  at zero temperature, given as

$$1 = \frac{2\pi\mu^2\lambda}{(2\pi\hbar v_F)^3} \ln \frac{\sqrt{\omega_D^2 + \Delta_F^2} + \omega_D}{\Delta_F}. \quad (10)$$

Because  $\mu \gg \omega_D$ , it is found  $\Delta_F = 2\omega_D \exp[-C/(\lambda\mu^2)]$  where  $C = 4\pi^2(\hbar v_F)^3$ . As the interaction strength increases, more electrons partake in pairing. As a result,  $\Delta_F$  increases with  $\lambda$ , shown by a blue dot-dashed curve in Figs. 2(a) and 2(b).

### B. BCS pairing

Equation (9) is reduced to

$$1 = \int_D \frac{d\mathbf{k}}{(2\pi\hbar)^3} \frac{(1+\alpha)\lambda \sin^2 \theta}{4\sqrt{(v_F k - \mu)^2 + \Delta_B^2 \sin^2 \theta}}. \quad (11)$$

The energy gap is found as  $\Delta_B = e^{5/6}\omega_D \exp\{-3C/[2(1+\alpha)\lambda\mu^2]\}$ . There are two limiting situations: when the electrons are scattered into the same Weyl node, corresponding to  $\alpha = 0$ , the energy gap is  $\Delta_B^{(1)} = e^{5/6}\omega_D \exp[-3C/(2\lambda\mu^2)]$ ; when the scattering is between different Weyl nodes with equal intensity, corresponding to  $\alpha = 1$ , the energy gap is  $\Delta_B^{(2)} = e^{5/6}\omega_D \exp[-3C/(4\lambda\mu^2)]$ . We plot the  $\lambda$  dependence of  $\Delta_B^{(1)}$  and  $\Delta_B^{(2)}$  by the green-dashed and the red curves in Fig. 2(a), respectively. That  $\Delta_B^{(1)}$  and  $\Delta_B^{(2)}$  increase with  $\lambda$  implies that the more pronounced electrons partake in the pairing. We also show the  $\alpha$  dependence of pairing potential  $\Delta_B$  by the red curve in Fig. 2(b). Increasing  $\alpha$  enhances the scattering from one Weyl node to another Weyl node and more electrons partake in the pairing.

### C. FFLO/BCS hybrid pairings

Equations (8) and (9) lead to

$$1 = \frac{\lambda\mu^2}{2C} \int d\theta \sin \theta \sum_v \frac{\Pi_v(\theta)}{2\Delta'_F} \ln \frac{2\omega_D}{|\Pi(\theta)|} \quad (12)$$

and

$$1 = \frac{\lambda(1+\alpha)\mu^2}{2C} \int d\theta \sin^2 \theta \sum_v \frac{v\Pi_v(\theta)}{2\Delta'_F} \ln \frac{2\omega_D}{|\Pi(\theta)|}, \quad (13)$$

where  $\Pi_v(\theta) = \Delta'_F + v\Delta'_B \sin \theta$  and  $v = \pm 1$ . The FFLO/BCS hybrid state is a local minimum solution of the mean-field thermodynamic potential. We show  $\Delta'_F$  and  $\Delta'_B$  by a blue short-dashed curve and a red long-dashed curve, respectively, in Fig. 2. There exists a critical value  $\lambda\mu^2/C = 1/4$  for the hybrid pairing. Below this value, the pairing tends to be the FFLO type.  $\Delta'_B = 0$  for  $\lambda\mu^2/C \leq 1/4$  so that  $\Delta'_F = \Delta_F$ . Conversely,  $\lambda\mu^2/C > 1/4$ ,  $\Delta'_B$  has nonzero value, while  $\Delta'_F$  decreases. Around  $\lambda\mu^2/C = 1/4$ ,  $\Delta'_B$  is much smaller in comparison to  $\Delta'_F$ ; we expand gap functions,  $(\lambda\mu^2/C)[\ln(2/\Delta'_F) - \Delta_B^2/(3\Delta_F^2)] = 1$  and  $2(\lambda\mu^2/C)\{(2/3)([\ln(2/\Delta'_F) - 1]) + 4\Delta_B^2/(45\Delta_F^2)\} = 1$ . The solutions are  $\Delta'_F = 2\omega_D \exp[-C/(\lambda\mu^2) - (1/3)(\Delta_B^2/\Delta_F^2)]$  and  $\Delta'_B = \Delta'_F \sqrt{15/7[1 - C/(4\lambda\mu^2)]}$ . From these,  $\Delta'_B = 0$  and  $\Delta'_F = 2\omega_D \exp[-C/(\lambda\mu^2)]$  when  $\lambda\mu^2/C = 1/4$ . When  $\lambda\mu^2/C > 1/4$ , both  $\Delta'_F$  and  $\Delta'_B$  are real and positive. When  $\mu^2/C < 1/4$ , there is no solution for the gap functions because  $\Delta'_F$  and  $\Delta'_B$  must be real and positive. As a consequence, no FFLO/BCS hybrid pairing is possible for  $\lambda\mu^2/C < 1/4$ . The minimum  $U$  required for the occurrence of the FFLO/BCS hybrid pairings in SWSMs is  $U_{min} = 4\pi^2(\hbar v_F)^3/\mu^2$ .

The variation of the FFLO/BCS hybrid pairing with  $\alpha$  is shown in Fig. 2(b). For  $\lambda\mu^2/C = 1/4$ , at small value  $\alpha$ , there is no solution for the FFLO/BCS hybrid pairing. As  $\alpha$  increases,  $\Delta'_B$  deviates gradually from  $\Delta_B$  and  $\Delta'_F$  increases from zero. At a large value of  $\alpha$ ,  $\Delta'_B$  vanished and  $\Delta'_F$  approaches  $\Delta_F$ . The FFLO/BCS hybrid pairing is only possible in a finite region of  $\alpha$ . The BCS state appears at a small  $\alpha$ ,

while the FFLO state appears at a large  $\alpha$ . The BCS pairing potential increases with  $\alpha$  in the case of pure BCS pairing. This indicates that electrons are in favor of internode scattering. On the contrary,  $\Delta'_B$  is suppressed with the mixing of  $\Delta'_F$ . Because the total electrons around the Fermi surface is fixed, the intranode pairing divides up the internode pairing. Therefore,  $\Delta'_B$  decreases as  $\alpha$  increases accordingly.

### V. CONDENSATION ENERGY

Because three pairing schemes can be energetically stabilized in a large region of  $\lambda$ , it is relevant to consider the nature of the ground state of these superconducting phases with different pairings. We evaluate the condensation energy with different pairings. The Hamiltonians  $H_I^F$  and  $H_I^B$  in the mean-field approximation are  $H_I^F = -(1/2) \sum_{\kappa} \int d\mathbf{k}/(2\pi\hbar)^3 \Delta_F (c_{\kappa, \mathbf{k}_{\kappa,+}}^{\dagger} + c_{\kappa, -\mathbf{k}_{\kappa,+}}^{\dagger} + \text{c.c.}) + \sum_{\kappa} \Delta_F^2/\lambda$  and  $H_I^B = -(1/2) \sum_{\kappa} \int d\mathbf{k}/(2\pi\hbar)^3 \Delta_B \sin \theta (c_{\kappa, \mathbf{k}_{\kappa,+}}^{\dagger} + c_{-\kappa, -\mathbf{k}_{\kappa,+}}^{\dagger} + \text{c.c.}) + \sum_{\kappa} \Delta_B^2/[(1+\alpha)\lambda]$ . Under the Bogoliubov transformation,  $\phi_{\kappa, v, +}(\mathbf{k}) = u_{\kappa, v, +}(c_{\kappa, \mathbf{k}_{\kappa,+}} + v c_{-\kappa, -\mathbf{k}_{\kappa,+}}) + v_{\kappa, v, +}(v c_{\kappa, \mathbf{k}_{\kappa,+}}^{\dagger} + c_{-\kappa, -\mathbf{k}_{\kappa,+}}^{\dagger})$  and  $\phi_{\kappa, v, +}^{\dagger}(\mathbf{k}) = u_{\kappa, v, +}(c_{\kappa, \mathbf{k}_{\kappa,+}}^{\dagger} + v c_{-\kappa, -\mathbf{k}_{\kappa,+}}^{\dagger}) + v_{\kappa, v, +}(v c_{\kappa, \mathbf{k}_{\kappa,+}} + c_{-\kappa, -\mathbf{k}_{\kappa,+}})$ , where  $u_{\kappa, v, +} = \sqrt{1 + (v_F k - \mu)/E_v(\mathbf{k})/2}$  and  $v_{\kappa, v, +} = (v\Delta_F + \Delta_B \sin \theta)/[2E_v(\mathbf{k})\sqrt{1 + (v_F k - \mu)/E_v(\mathbf{k})}]$ , the Hamiltonian can be diagonalized, given as

$$H = \sum_{\kappa, v} \int \frac{d\mathbf{k}}{(2\pi\hbar)^3} E_v(\mathbf{k}) \phi_{\kappa, v, +}^{\dagger}(\mathbf{k}) \phi_{\kappa, v, +}(\mathbf{k}) + E(\Delta_F, \Delta_B),$$

where

$$E(\Delta_F, \Delta_B) = \sum_{\kappa, v=\pm 1} \int \frac{d\mathbf{k}}{(2\pi\hbar)^3} \frac{(v_F k - \mu) - E_v(k)}{2} + \Lambda_{\alpha},$$

$\Lambda_{\alpha} = \sum_{\kappa} \Delta_F^2/\lambda + \sum_{\kappa} \Delta_B^2/[(1+\alpha)\lambda]$ , and  $E_v(k)$  is the eigenenergy for the Bogoliubov quasiparticles. The condensation energy  $E^C$  is defined by  $E^C = E(\Delta_F, \Delta_B) - E(0, 0)$  [31]. Below we can evaluate  $E^C$  at zero temperature.

(a) Pure FFLO pairing: The eigenenergy is  $E^F(\mathbf{k}) = \sqrt{(v_F k - \mu)^2 + \Delta_F^2}$ . The condensation energy is found as

$$E_F^C = -\frac{8\omega_D^2 \mu^2}{C} e^{-2C/\lambda\mu^2} \left[ \ln\left(\frac{\mu}{\omega_D}\right) - 1 \right]. \quad (14)$$

(b) Pure BCS-type: The eigenenergy is  $E^B(\mathbf{k}) = \sqrt{(v_F k - \mu)^2 + \Delta_B^2 \sin^2 \theta}$ . Then condensation energy is found as

$$E_B^C(\alpha) = -\frac{4e^{5/3}\mu^2\omega_D^2}{3C} e^{-[3C/(1+\alpha)\lambda\mu^2]} \left( \ln\frac{\mu}{\omega_D} - 1 \right). \quad (15)$$

$E_B^C(0)$  corresponds to intranode scattering while  $E_B^C(1)$  corresponds to internode scattering.

(c) FFLO/BCS hybrid pairings: Due to two branches  $E_v(\mathbf{k})$  with  $v = \pm$ , there are two effective energy gaps,  $\Delta_{\text{eff}}^v = |\Delta_F + v\Delta_B \sin \theta|$ . The FFLO and BCS pairings are coupled. The condensation energy is found as

$$E_M^C = \frac{2\mu^2}{C} \sum_v \int_0^{\pi} d\theta \sin \theta \Delta_{\text{eff}}^{v,2} \left( 1 - \ln \frac{2\mu}{\Delta_{\text{eff}}^v} \right) + \Lambda_{\alpha}. \quad (16)$$

We show  $E_F^C$ ,  $E_B^C = E_B^C(0) + E_B^C(1)$ , and  $E_M^C$  in Figs. 2(c) and 2(d) by a blue dot-dashed, solid red, and magenta dashed curves, respectively. From Fig. 2(c), it is found that if the electron is scattered within the same Weyl node ( $\alpha = 0$ ), the FFLO state should be the ground state in the SWSM, which corresponds with that given by Moore *et al.* [9]. However, if the electrons can be scattered at both nodes ( $\alpha = 1$ ), the ground state is a BCS state, which corresponds to that given by Burkov [13]. For  $\lambda\mu^2/C = 1/4$ , Fig. 2(d) shows that the FFLO state is the ground state for small  $\alpha$ , while the BCS state is the ground state for large  $\alpha$ . We found that the condensation energy with the FFLO/BCS hybrid pairings is always higher than those with the pure FFLO and BCS pairings.

Under FFLO/BCS hybrid pairing, the gap equation is determined by Eqs. (12) and (13) simultaneously. There are two solutions, with effective gaps of  $|\Delta_B' \pm \Delta_F'|$ . The state with a large gap is more stable than the one with a small gap. We calculated the condensation energy of the BCS state, the FFLO state, and the hybrid pairing state with a large gap. The results show that the condensation energy of the hybrid pairing state is higher than that of the pure BCS and FFLO pairing state in the whole parameter range. The reason for this is the following. In the mixed pairing, internode and intranode coexist. The pure BCS and FFLO paired states are perfectly ordered ground states. Mixed pairing results in entangled states and removes the perfect ordering, or the state is slightly disordered due to the pairing mixing. In this case the ground state energy is always higher than that under a pure pairing.

We conclude that a state with a hybrid pairing cannot be a ground state.

## VI. CONCLUSION

In SWSMs, there are three possible pairings: FFLO, BCS, and FFLO/BCS hybrid pairing. The nature of the electron scattering determines which pairing is favored. If the intranode scattering is dominant, the ground state is with the FFLO pairing. If the internode scattering is strong, the ground state is with a BCS pairing. This reflects the fact that more electrons can be paired. More generally, when the electron scattering between two Weyl nodes is weak, the FFLO phase is the ground state. Because the energy spectrum with a FFLO pairing is fully gapped, the BCS pairing is suppressed. However, if the inter-node scattering is strong enough, the ground state is in favour of the BCS pairing. Two effective gaps coexist in the case of the FFLO/BCS hybrid pairing. From the condensation energy, we found that although the state with the FFLO/BCS hybrid pairing exists, it cannot be the ground state of SWSM. Our result has resolved the issue of whether a state with FFLO/BCS hybrid pairing can be the ground state of SWSM.

## ACKNOWLEDGMENTS

The authors are thankful for the support of NSFC (Grants No. 11274013 and No. 11774006), NBRP of China (Grant No. 2012CB921300), and the Australian Research Council (Grant No. DP210101436).

- 
- [1] S. Murakami, Phase transition between the quantum spin Hall and insulator phases in 3D: Emergence of a topological gapless phase, *New J. Phys.* **9**, 356 (2007).
- [2] X. Wan, A. M. Turner, A. Vishwanath, and S. Y. Savrasov, Topological semimetal and Fermi-arc surface states in the electronic structure of pyrochlore iridates, *Phys. Rev. B* **83**, 205101 (2011).
- [3] A. A. Burkov and L. Balents, Weyl Semimetal in a Topological Insulator Multilayer, *Phys. Rev. Lett.* **107**, 127205 (2011).
- [4] S.-M. Huang, S.-Y. Xu, I. Belopolski, C.-C. Lee, G. Chang, B. K. Wang, N. Alidoust, G. Bian, M. Neupane, C. Zhang, S. Jia, A. Bansil, H. Lin, and M. Hasan, A Weyl Fermion semimetal with surface Fermi arcs in the transition metal monopnictide TaAs class, *Nat. Commun.* **6**, 7373 (2015).
- [5] B. Q. Lv, H. M. Weng, B. B. Fu, X. P. Wang, H. Miao, J. Ma, P. Richard, X. C. Huang, L. X. Zhao, G. F. Chen, Z. Fang, X. Dai, T. Qian, and H. Ding, Experimental Discovery of Weyl Semimetal TaAs, *Phys. Rev. X* **5**, 031013 (2015).
- [6] B. Q. Lv, N. Xu, H. M. Weng, J. Z. Ma, P. Richard, X. C. Huang, L. X. Zhao, G. F. Chen, C. E. Matt, F. Bisti, V. N. Strocov, J. Mesot, Z. Fang, X. Dai, T. Qian, M. Shi, and H. Ding, Observation of Weyl nodes in TaAs, *Nat. Phys.* **11**, 724 (2015).
- [7] H. M. Weng, C. Fang, Z. Fang, B. A. Bernevig, and X. Dai, Weyl Semimetal Phase in Noncentrosymmetric Transition-Metal Monophosphides, *Phys. Rev. X* **5**, 011029 (2015).
- [8] S.-Y. Xu, I. Belopolski, N. Alidoust, M. Neupane, G. Bian, C. Zhang, R. Sankar, G. Chang, Z. Yuan, C.-C. Lee, S.-M. Huang, H. Zheng, J. Ma, D. S. Sanchez, B. Wang, A. Bansil, F. Chou, P. P. Shibayev, H. Lin, S. Jia *et al.*, Discovery of a Weyl fermion semimetal and topological Fermi arcs, *Science* **349**, 613 (2015).
- [9] G. Y. Cho, J. H. Bardarson, Y.-M. Lu, and J. E. Moore, Superconductivity of doped Weyl semimetals: Finite-momentum pairing and electronic analog of the  $^3\text{He-A}$  phase, *Phys. Rev. B* **86**, 214514 (2012).
- [10] H. Wei, S.-P. Chao, and V. Aji, Odd-parity superconductivity in Weyl semimetals, *Phys. Rev. B* **89**, 014506 (2014).
- [11] T. Meng and L. Balents, Weyl superconductors, *Phys. Rev. B* **86**, 054504 (2012).
- [12] S. A. Yang, H. Pan, and F. Zhang, Dirac and Weyl Superconductors in Three Dimensions, *Phys. Rev. Lett.* **113**, 046401 (2014).
- [13] G. Bednik, A. A. Zyuzin, and A. A. Burkov, Superconductivity in Weyl metals, *Phys. Rev. B* **92**, 035153 (2015).
- [14] Y. Qi, P. G. Naumov, M. N. Ali, Ca. R. Rajamathi, W. Schnelle, O. Barkalov, M. Hanfland, S.-C. Wu, C. Shekhar, Y. Sun, V. Süß, M. Schmidt, U. Schwarz, E. Pippel, P. Werner, R. Hillebrand, T. Förster, E. Kampert, S. Parkin, R. J. Cava, C. Felser *et al.*, Superconductivity in Weyl semimetal candidate  $\text{MoTe}_2$ , *Nat. Commun.* **7**, 11038 (2016).
- [15] T. Zhou, Y. Gao, and Z. D. Wang, Superconductivity in doped inversion-symmetric Weyl semimetals, *Phys. Rev. B* **93**, 094517 (2016).
- [16] Y. Li and F. D. M. Haldane, Topological Nodal Cooper Pairing in Doped Weyl Metals, *Phys. Rev. Lett.* **120**, 067003 (2018).

- [17] B. Lu, K. Yada, M. Sato, and Y. Tanaka, Crossed Surface Flat Bands of Weyl Semimetal Superconductors, *Phys. Rev. Lett.* **114**, 096804 (2015).
- [18] P. Fulde and R. A. Ferrell, Superconductivity in a Strong Spin-Exchange Field, *Phys. Rev.* **135**, A550 (1964).
- [19] A. Larkin and Y. N. Ovchinnikov, Nonuniform state of superconductors, *Sov. Phys. JETP* **20**, 762 (1965).
- [20] D. F. Agterberg and R. P. Kaur, Magnetic-field-induced helical and stripe phases in Rashba superconductors, *Phys. Rev. B* **75**, 064511 (2007).
- [21] G. Volovik, Flat band in the core of topological defects: Bulk-vortex correspondence in topological superfluids with Fermi points, *JETP Lett.* **93**, 66 (2011).
- [22] Y. Sun, S.-C. Wu, M. N. Ali, C. Felser, and B. Yan, Prediction of Weyl semimetal in orthorhombic  $\text{MoTe}_2$ , *Phys. Rev. B* **92**, 161107(R) (2015).
- [23] A. A. Zyuzin, S. Wu, and A. A. Burkov, Weyl semimetal with broken time reversal and inversion symmetries, *Phys. Rev. B* **85**, 165110 (2012).
- [24] W. Chen, L. Jiang, R. Shen, L. Sheng, B. Wang, and D. Xing, Specular Andreev reflection in inversion-symmetric Weyl semimetals, *Europhys. Lett.* **103**, 27006 (2013).
- [25] J. Fang, W. Duan, J. Liu, C. Zhang, and Z. Ma, Pairing-dependent superconductivity gap and nonholonomic Andreev reflection in Weyl semimetal/Weyl superconductor heterojunctions, *Phys. Rev. B* **97**, 165301 (2018).
- [26] W. Y. Duan, J. F. Liu, J. Fang, C. Zhang, and Z. S. Ma, Transverse conductance in a three-dimensional Weyl semimetal and Weyl superconductor hybrid under a strong magnetic field, *Phys. Rev. B* **98**, 155317 (2018).
- [27] Y. Kim, M. J. Park, and M. J. Gilbert, Probing unconventional superconductivity in inversion-symmetric doped Weyl semimetal, *Phys. Rev. B* **93**, 214511 (2016).
- [28] S. Uddin, W. Y. Duan, J. Wang, Z. S. Ma, and J.-F. Liu, Chiral anomaly induced oscillations in the Josephson current in Weyl semimetals, *Phys. Rev. B* **99**, 045426 (2019).
- [29] M. J. Park, J. Yang, Y. Kim, and M. J. Gilbert, Fulde-Ferrell states in inverse proximity-coupled magnetically doped topological heterostructures, *Phys. Rev. B* **96**, 064518 (2017).
- [30] G. D. Mahan, *Many-Particle Physics*, 3rd ed. (Plenum, New York, 2013).
- [31] P. G. de Gennes, *Superconductivity of Metals and Alloys* (Perseus books, Reading, MA, 1999).